Journal of Magnetism and Magnetic Materials 471 (2019) 334–339

Contents lists available at ScienceDirect

Journal of Magnetism and Magnetic Materials

journal homepage: www.elsevier.com/locate/jmmm

Research articles

Effect of viscosity on the AC magnetization of magnetic nanoparticles under different AC excitation fields

Takashi Yoshida*, Takuru Nakamura, Oji Higashi, Keiji Enpuku

Department of Electrical and Electronic Engineering, Kyushu University, Fukuoka 819-0395, Japan

ARTICLE INFO

Keywords:
Magnetic nanoparticle
Viscosity
Field dependent relaxation
Magnetic fluid hyperthermia
Magnetic particle imaging

ABSTRACT

For *in vivo* applications of magnetic nanoparticles (MNPs), environment viscosity is one of the most important parameters that determines their AC magnetization. In this study, we investigate the effect of viscosity on the AC magnetization of MNPs under different AC excitation field conditions. We show that the AC $M-H$ curve and harmonic magnetization spectrum strongly depend on the viscosity for a small excitation field intensity and low excitation frequency, while they are insensitive to the viscosity for a large excitation field intensity and high excitation frequency. We then show that the difference in the AC magnetization between these cases can be qualitatively explained by taking the field dependent Brownian $f_B(H_{ac})$ and Néel $f_N(H_{ac})$ frequencies into account. The frequencies are obtained from numerical simulations based on the Fokker-Planck equations. Finally, we show that an excitation field with a relatively large intensity and a frequency f that satisfies $f_B(H_{ac}) \ll f \leq f_N(H_{ac})$ is suitable for the magnetic fluid hyperthermia (MFH) application.

1. Introduction

Magnetic nanoparticles (MNPs) have been widely studied because of their potential use in biomedical applications such as magnetic fluid hyperthermia (MFH) and magnetic particle imaging (MPI) [1–3]. These applications make use of the dynamic magnetization of MNPs under an AC excitation field. It has been shown that the dynamic magnetization is affected by MNP parameters such as the magnetic moment m, anisotropy energy E, particle size distribution, and the frequency and intensity of the AC excitation field [4–7]. Studies have been performed to characterize the dynamic magnetization of both suspended and immobilized MNPs [4–7].

For in vivo applications of MNPs, the viscous environment is a critical factor that determines the AC magnetization. Therefore, the effect of the viscosity on the AC magnetization has been studied for biomedical applications such as MFH and MPI [8–13]. Ota et al. measured the AC magnetizations (hysteresis loops) of MNP suspensions with different viscosities to understand the effect of Brownian rotation, which is related to the viscosity [8]. They concluded that the Brownian rotation affected the intrinsic loss power (ILP), even though Néel relaxation was faster than Brownian relaxation. Shasha et al. investigated the effect of both nanoparticle size and viscosity on third harmonic magnetization, which is used in MPI as a detection signal [9].

In this study, we investigated the effect of viscosity on the AC magnetization of MNPs. To this end, we prepared three MNP samples with different viscosities. We measured the AC magnetization and harmonic magnetization spectra from each sample under different AC excitation field conditions. To understand the differences in the AC magnetization among the three samples, we performed a numerical simulation based on the Fokker-Planck equation. From these results, we discussed how the viscosity and the excitation field condition affected the magnetization mechanism. Furthermore, we determined the appropriate excitation field condition for MFH.

2. Materials and methods

2.1. Core and hydrodynamic sizes of MNPs

Commercial Resovist® MNPs (FUJIFILM RI Pharma, Japan) is a hydrophilic colloidal solution of Fe_3O_4/γ–Fe_2O_3 nanoparticles coated with carboxydextran, with primary core diameters of 5–10 nm. Resovist® consists of elementary particles with a small magnetic moment and multi-core particles with a large magnetic moment [14,15]. Since an MNP sample with a large magnetic moment and narrow size distribution is suitable for biomedical applications such as MFH and MPI, a magnetically fractionated Resovist® sample was prepared. The magnetic fractionation method is described elsewhere [16,17].

The core size distribution of the fractionated Resovist® sample,

* Corresponding author.
E-mail address: t_yoshi@ees.kyushu-u.ac.jp (T. Yoshida).

https://doi.org/10.1016/j.jmmm.2018.09.127
Received 24 June 2018; Received in revised form 24 September 2018; Accepted 30 September 2018
Available online 02 October 2018
0304-8853/

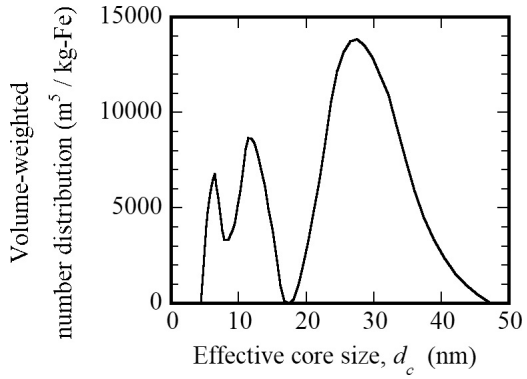

Fig. 1. Effective core size distribution of the MNP sample. The distribution was estimated from the static $M - H$ curve.

which was estimated from the static $M - H$ curve [18–20], is shown in Fig. 1(a). The typical core size of the fractionated Resovist® sample was 27.5 nm. We also found that the fraction of MNPs with a small core size was small, indicating that the fractionated Resovist® sample mainly consisted of MNPs with a large core size (i.e., a large magnetic moment). Note that the portion of MNPs with a large core size in the original Resovist® sample was only about 30% in terms of the volume-weighted number distribution [4]. The z-averaged hydrodynamic diameter and polydispersity index (PDI) of the sample, which were measured with a dynamic light scattering setup (Zetasizer Nano ZS, Malvern Instruments), were 60.5 nm and 0.18, respectively.

2.2. Sample preparation

To investigate the effect of the viscosity of the MNP sample solution on the AC magnetization properties, we prepared three samples (S1–S3) with different viscosities by diluting the water-based fractionated Resovist® suspension with different volumes of glycerol, as shown in Table 1. The iron concentration and volume of each sample was adjusted to be 1 μg-Fe/μL and 150 μl, respectively. The calculated viscosity values [21] of the three samples at a room temperature $T = 297$ K were η = 0.957 mPa•s, 9.43 mPa•s, and 411 mPa•s for sample S1, S2, and S3, respectively, as listed in Table 1.

2.3. AC magnetization measurements

An AC excitation field with frequency f, expressed as $H(t) = H_{ac}\cos(2\pi ft)$, was applied using a solenoid coil to measure the dynamic magnetization of the three samples. The magnetic signal from the MNPs was detected using an inductive pickup coil. The derivative of $M(t)$, i.e., $dM(t)/dt$ was proportional to the voltage across the pickup coil, while the dynamic magnetization $M(t)$ of the sample was obtained by integrating the voltage across the pickup coil. In doing so, the conversion coefficient was calculated using the reciprocity principle [22]. Harmonic magnetization signals were calculated from the Fourier transform of $M(t)$. Details of the measurement system were previously published [23].

Table 1
Three samples with different volumes of water-based MNP suspension and glycerol. The viscosity of each sample was calculated from Ref. [21].

	Volume of water-based MNPs (μl)	Volume of glycerol (μl)	Viscosity (mPa•s)
S1	150	0	0.957
S2	70	80	9.43
S3	10	140	411

2.4. Numerical simulations

To derive the field dependent Brownian and Néel relaxation times, we performed numerical simulations based on the Fokker–Planck equations. In this study, we derived the field dependent relaxation times for typical core and hydrodynamic sizes of MNP.

For the Brownian magnetization mechanism, the dynamic magnetization behavior is given by the following equation [24]

$$2\tau_B \frac{\partial W}{\partial t} = \frac{1}{\sin\theta}\frac{\partial}{\partial\theta}\left[\sin\theta\left(\xi\sin\theta \bullet W + \frac{\partial W}{\partial\theta}\right)\right]. \quad (1)$$

Here, θ is the angle of the magnetic moment m of the MNP with respect to the applied field $H(t)$, $W(\theta, t)$ is the probability density of the orientation of the magnetic moment, $\xi(t) = \mu_0 mH(t)/k_B T$ is the external field energy normalized by the thermal energy, and k_B is the Boltzmann constant. $\tau_B = \pi\eta d_H^3/2k_B T$ is the Brownian relaxation time with zero field, where η is the viscosity and d_H is the hydrodynamic size of the MNP. As shown in Eq. (1), Fokker–Planck equation represents the dynamic behavior of probability density.

For the Néel magnetization mechanism, we assumed uniaxial anisotropy with the easy axis direction parallel to the external field for simplicity, though the angle of the easy axis of the MNP with respect to the external field should be taken into account in general to simulate the Néel magnetization [25]. In this case, the dynamic magnetization behavior is given by the following equation [24]

$$2\tau_N \frac{\partial W}{\partial t} = \frac{1}{\sin\theta}\frac{\partial}{\partial\theta}\left\{\sin\theta\left[(\xi\sin\theta + \sigma\sin 2\theta)W + \frac{\partial W}{\partial\theta}\right]\right\}. \quad (2)$$

Here, $\tau_{N0} = \tau_N/\sigma = 10^{-9}$ is the characteristic Néel relaxation time, $\sigma = \pi K d_c^3/6k_B T$ is the anisotropy energy barrier normalized by $k_B T$, K is the anisotropy constant, and d_c is the core size of the MNP.

By solving the Fokker-Planck equations for both the Brownian and Néel mechanisms given in Eqs. (1) and (2), respectively, the fundamental components of the real and imaginary parts of the magnetization can be numerically calculated. For the calculations of Eqs. (1) and (2), we used the matrix continued fraction technique [26]. In the numerical calculations, we assumed that all MNPs had the same core size and hydrodynamic size for simplicity. We set the core and hydrodynamic sizes to $d_c = 27.5$ nm and $d_H = 60.5$ nm, respectively. In this case, the magnetic moment of the MNP was calculated as $m = \frac{M_s \pi d_c^3}{6} = 3.54 \times 10^{-18}\mathrm{Am}^2$ for $M_s = 325.5$ kA/m, which was obtained from the static $M - H$ curve.

3. Results

3.1. AC $M - H$ curve

Fig. 2 shows the measured AC $M - H$ curves of samples S1–S3 for each AC excitation field condition. As shown in Fig. 2(a), the AC $M - H$ curves were different when the excitation field was $\mu_0 H_{ac} = 3.5$ mT and $f = 3$ kHz. This result indicates that in this case the AC $M - H$ curves strongly depended on the viscosity. Since the viscosity affects the Brownian mechanism, the results shown in Fig. 2(a) mean that the Brownian mechanism affects the AC magnetization under this AC field condition.

When the excitation frequency was increased to $f = 20$ kHz at $\mu_0 H_{ac} = 3.5$ mT, the maximal magnetization of S1 became smaller compared with the case of $f = 3$ kHz, as shown in Fig. 2(b). Under these conditions, the differences in the AC $M - H$ curves among the three samples became smaller compared with the case of $f = 3$ kHz.

Under a large excitation field of $\mu_0 H_{ac} = 20$ mT, the AC $M - H$ curves were almost the same for all three samples, as shown in Fig. 2(c) ($f = 3$ kHz) and 2(d) ($f = 20$ kHz). These results indicate that the AC $M - H$ curves were insensitive to the viscosity. Namely, the effect of the Brownian mechanism on the AC $M - H$ curves reduced when the

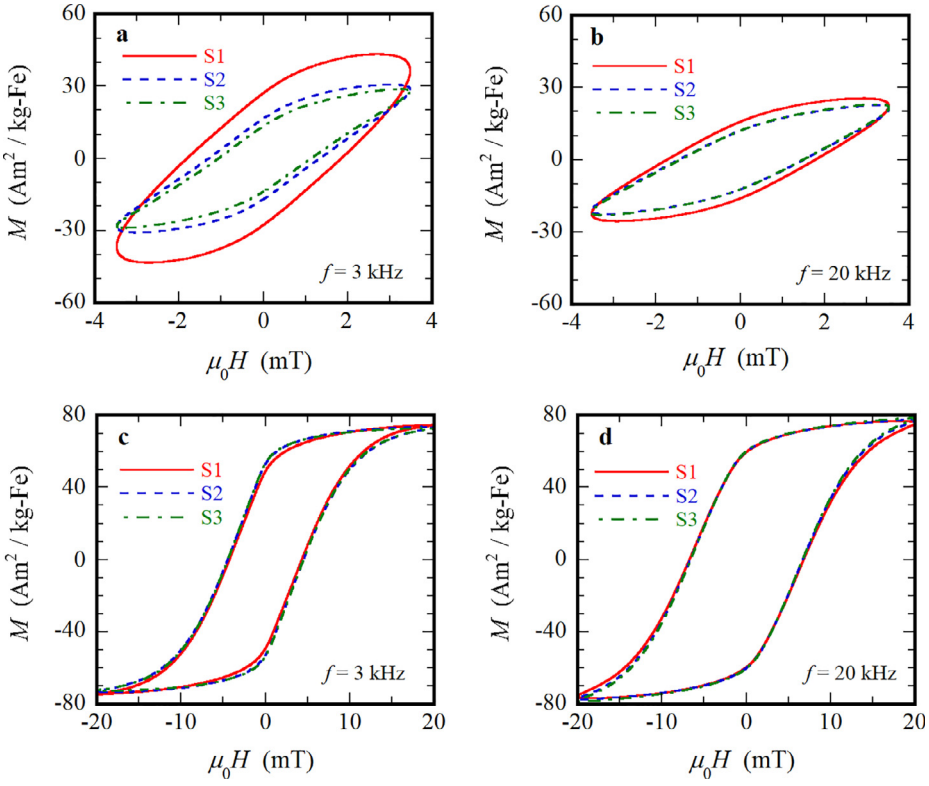

Fig. 2. $M - H$ curves of three samples under different AC excitation fields. (a) $\mu_0 H_{ac}$ = 3.5 mT and f = 3 kHz, (b) $\mu_0 H_{ac}$ = 3.5 mT and f = 20 kHz, (c) $\mu_0 H_{ac}$ = 20 mT and f = 3 kHz, and (d) $\mu_0 H_{ac}$ = 20 mT and f = 20 kHz.

amplitude of the excitation field increased.

Fig. 3 shows the dependence of the hysteresis loop area A on the viscosity for each AC excitation field condition. The vertical axis represents the hysteresis loop area normalized by the area of S1. As shown by the open rectangles, the area was strongly affected by the viscosity when $\mu_0 H_{ac}$ = 3.5 mT and f = 3 kHz. The areas of S2 and S3 were 55% and 43%, respectively, of the area of S1. However, the area was almost insensitive to the viscosity for the excitation field $\mu_0 H_{ac}$ = 20 mT and f = 20 kHz, as shown by the closed rectangles in Fig. 3. The areas of S2 and S3 were 97% and 98%, respectively, of the area of S1.

3.2. $dM/dt - H$ curve

Fig. 4 shows the $dM/dt - H$ curves of samples S1–S3 for each AC excitation field condition. By convention, only half of the full period, i.e., forward scan with respect to H, is shown. Note that, the height and width of the $dM/dt - H$ correspond to the sensitivity and spatial resolution, respectively, in x-space MPI. The heights of $dM/dt - H$ curves for $\mu_0 H_{ac}$ = 3.5 mT were small compared to those for $\mu_0 H_{ac}$ = 20 mT. This means that the magnetization does not saturate under the AC excitation field amplitude of 3.5 mT. From Fig. 4(c) and (d), it is also found that the width of the $dM/dt - H$ curve for 20 kHz became slightly broader compare to that for 3 kHz. This will be caused by the finite relaxation time of MNP.

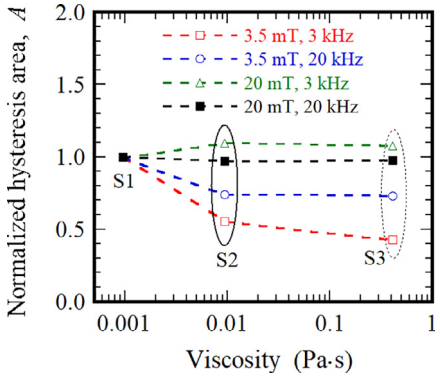

Fig. 3. Dependence of hysteresis loop area on the viscosity for different excitation field conditions. The vertical axis represents the hysteresis loop area normalized by the area of S1.

As in the case of AC $M - H$ curves, $dM/dt - H$ curves were affected by the viscosity as shown in Fig. 4(a). On the other hand, when the amplitude and frequency are large, $dM/dt - H$ curve is almost insensitive to the viscosity.

3.3. Harmonic magnetization

Fig. 5 shows the harmonic magnetization spectra for excitation field conditions of ($\mu_0 H_{ac}$, f) = (3.5 mT, 3 kHz) and (20 mT, 20 kHz). Note that, the harmonic magnetizations are used to reconstruct an MPI image in *frequency*-space MPI. The harmonic magnetization spectra of the three samples were different for the case of $\mu_0 H_{ac}$ = 3.5 mT and f = 3 kHz, indicating that the viscosity affected the harmonic spectra. However, the differences in the harmonic magnetization spectra between the three samples were negligible for the case of $\mu_0 H_{ac}$ = 20 mT and f = 20 kHz.

Fig. 6 shows the dependence of the third harmonic magnetization M_3 on the viscosity for each AC excitation field condition. Note that the vertical axis represents the third harmonic magnetization normalized by the value for S1. As shown by the open rectangles, the value of M_3 was strongly affected by the viscosity for the case of $\mu_0 H_{ac}$ = 3.5 mT and f = 3 kHz. The values of M_3 for S2 and S3 increased to 124% and 125%, respectively, of the value of S1. However, the value of M_3 was insensitive to the viscosity for the case of $\mu_0 H_{ac}$ = 20 mT and f = 20 kHz. The values of M_3 for S2 and S3 were 104% and 105%,

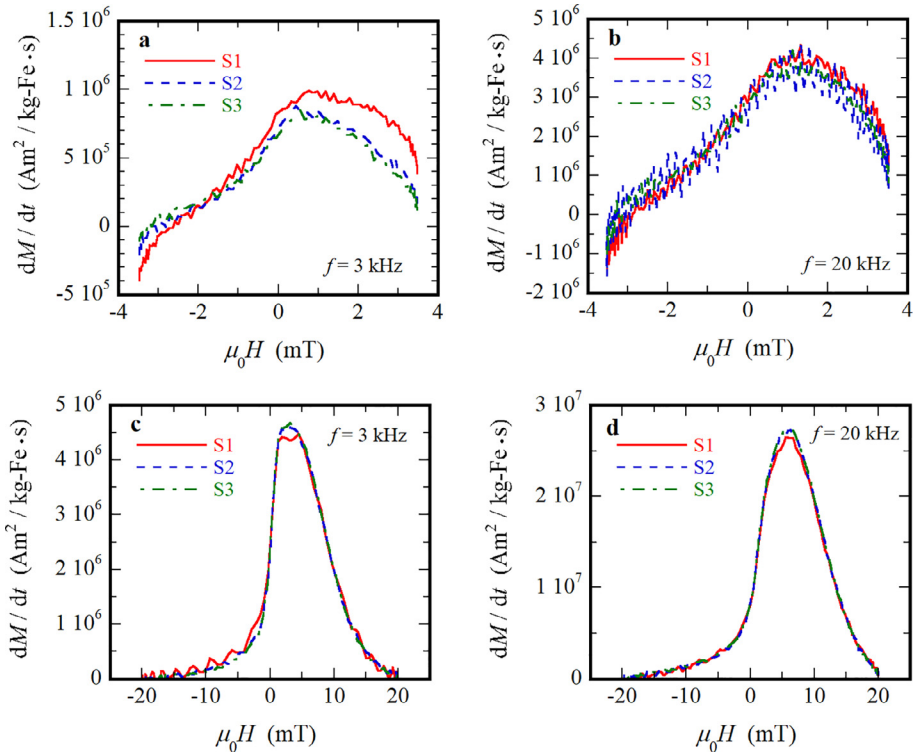

Fig. 4. dM/dt – H curves of three samples under different AC excitation fields. (a) $\mu_0 H_{ac}$ = 3.5 mT and f = 3 kHz, (b) $\mu_0 H_{ac}$ = 3.5 mT and f = 20 kHz, (c) $\mu_0 H_{ac}$ = 20 mT and f = 3 kHz, and (d) $\mu_0 H_{ac}$ = 20 mT and f = 20 kHz.

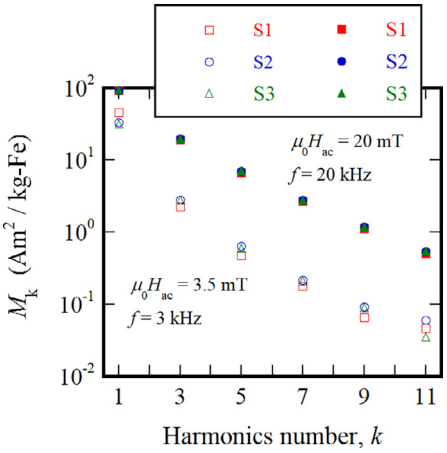

Fig. 5. Harmonic magnetization spectra. Open and filled symbols represent the harmonic magnetization spectra for excitation fields of ($\mu_0 H_{ac}$, f) = (3.5 mT, 3 kHz) and (20 mT, 20 kHz), respectively.

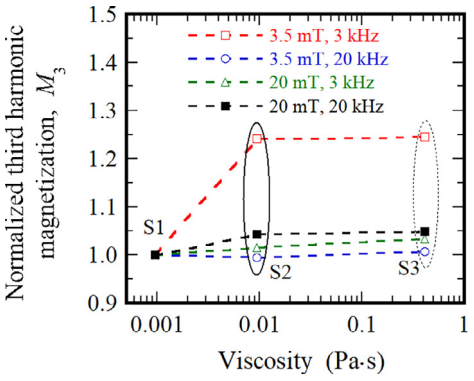

Fig. 6. Dependence of the third harmonic magnetization on the viscosity for different excitation field conditions. The vertical axis represents the third harmonic magnetization normalized by the value for S1.

respectively, of the value for S1.

3.4. Field dependent relaxation times

Fig. 7(a) shows the fundamental components of the real M_1' and imaginary M_1'' parts of the magnetization via the Brownian magnetization mechanism when the MNP sample is suspended in pure water, i.e., η = 0.957mPa•s. M_1'' was maximum at a frequency f_p. Here, we define the field dependent Brownian relaxation time as $\tau_B(H_{ac}) = 1/2\pi f_p$ and the field dependent Brownian frequency as $f_B(H_{ac}) = f_p$. As shown in Fig. 7(a), $f_B(H_{ac})$ shifted to the high frequency side when H_{ac} became large.

The field dependent Brownian frequency of S1 was $f_B(H_{ac})$ = 2.6 kHz and 8.3 kHz for $\mu_0 H_{ac}$ = 3.5 mT and 20 mT, respectively. Since the field dependent relaxation time is simply proportional to the viscosity of the suspension, f_B values for S2 and S3 were calculated using the viscosities listed in Table 1. We obtained f_B(3.5 mT/μ_0) = 0.26 kHz and f_B(20 mT/μ_0) = 0.84 kHz for S2 and f_B(3.5 mT/μ_0) = 0.0061 kHz and f_B(20 mT/μ_0) = 0.019 kHz for S3.

Fig. 7(b) shows the fundamental components of the real M_1' and imaginary M_1'' parts of the magnetization via the Néel magnetization mechanism. In the calculation, we set K = 6 kJ/m^3, which is typical of Resovist® particles [20,27,28]. As in the case of the Brownian magnetization mechanism, M_1'' was maximum at a certain frequency. In the same manner as the Brownian magnetization mechanism, we defined the field dependent Néel frequency $f_N(H_{ac})$. The field dependent Néel frequency of all samples was calculated as $f_N(H)$ = 0.29 kHz and 650 kHz for $\mu_0 H_{ac}$ = 3.5 mT and 20 mT, respectively. The $f_N(H)$ values were the same for all three samples.

By changing the amplitude of the excitation field H_{ac}, dependencies of Brownian $f_B(H_{ac})$ and Néel $f_N(H_{ac})$ frequencies on H_{ac} can be

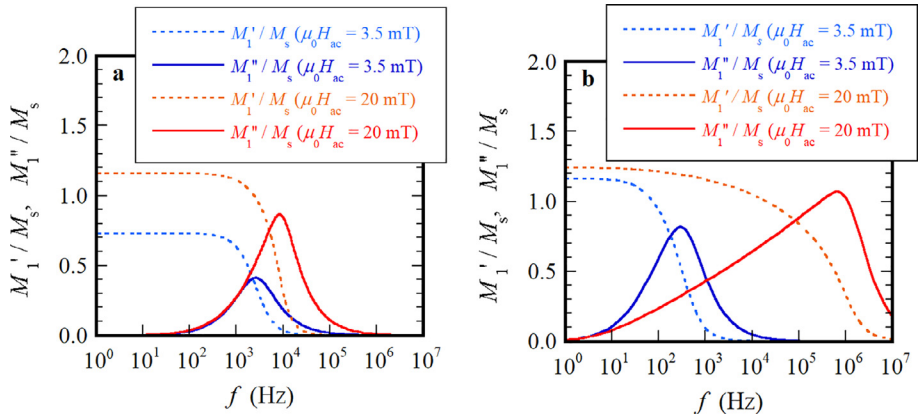

Fig. 7. Frequency dependence of the real M'/M_s and imaginary M''/M_s parts of the magnetization via (a) Brownian and (b) Néel mechanisms. The viscosity η = 0.957mPa•s was used in (a).

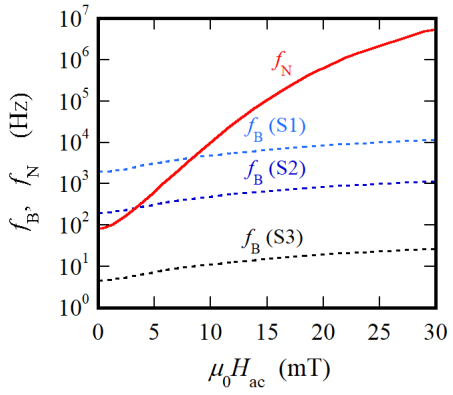

Fig. 8. Calculated field dependent Brownian $f_B(H_{ac})$ and Néel $f_N(H_{ac})$ frequencies. Results of f_B are shown for all three samples.

calculated as shown in Fig. 8.

4. Discussion

The parameters characterizing the AC magnetization properties of the three samples are summarized in Table 2. The obtained parameters were different among the three samples when $\mu_0 H_{ac}$ = 3.5 mT and f = 3 kHz. In this case, therefore, the parameters were affected by the viscosity. However, parameter differences among the three samples were small when the amplitude and frequency of the excitation field became large. In this case, therefore, the parameters were insensitive to the viscosity. We note that insensitiveness of the hysteresis loop area to the viscosity will be useful for the MFH application because the hysteresis loss (or specific absorption rate (SAR) value) is not affected by the environment viscosity. Similarly, insensitiveness of the dM/dt – H curve and harmonic spectra to the viscosity is useful for the MPI application because the MPI signal is not affected by the environment viscosity if the MNP environment such as aggregation can be ignored.

To understand the dynamic magnetization mechanism for different viscosities and field conditions, we discuss the field dependent Brownian and Néel frequencies shown in Fig. 8.

First, we considered the case of $\mu_0 H_{ac}$ = 3.5 mT. It was found that $f_B(S1) \gg f_N$, which indicates that the Brownian magnetization dominated for S1. For S2, $f_B(S2)$ and f_N were comparable, indicating that both the Brownian and Néel magnetizations were responsible for S2. For S3, $f_B(S3) \ll f_N$, therefore the Néel magnetization mechanism dominated for S3. Therefore, the AC $M - H$ curve and harmonic magnetization strongly depend on the viscosity for the excitation field $\mu_0 H_{ac}$ = 3.5 mT and f = 3 kHz, as shown in Figs. 2(a) and 4.

We note that $f > f_B$ and $f > f_N$ when the excitation field $\mu_0 H_{ac}$ = 3.5 mT and f = 20 kHz. In this case, the magnetic moment of the MNP can barely respond to the excitation field. As a result, the AC $M - H$ curve of S1 sample becomes much smaller than the case of f = 3 kHz, as shown in Fig. 2(b).

Next, we considered the case of $\mu_0 H_{ac}$ = 20 mT. As shown in Fig. 7, $f_N \gg f_B$ for all three samples. This result indicates that the Néel magnetization dominated for all samples. As a result, the AC $M - H$ curve and harmonic magnetization do not depend on the viscosity for the excitation field $\mu_0 H_{ac}$ = 20 mT, as shown in Figs. 2(c), (d), 4 and 5.

Finally, we discuss the appropriate excitation field condition for MFH. We note that the SAR value in MFH is related to M_1'' as

Table 2
Summary of ac magnetization properties. The values of area of hysteresis loop A, coercive field H_c, remanence M_r, and the intensity of the third harmonic magnetization M_3 under different excitation conditions (a) $\mu_0 H_{ac}$ = 3.5 mT and (b) $\mu_0 H_{ac}$ = 20 mT are shown.

(a) $\mu_0 H_{ac}$ = 3.5 mT	A (J/kg-Fe)		$\mu_0 H_c$ (mT)		M_r (Am^2/kg-Fe)		M_3 (Am^2/kg-Fe)	
	3 kHz	20 kHz	3 kHz	20 kHz	3 kHz	20 kHz	3 kHz	20 kHz
S1	0.274	0.156	1.84	1.77	27.2	15.9	2.24	1.55
S2	0.152	0.115	1.33	1.49	16.6	12.0	2.78	1.54
S3	0.117	0.114	1.13	1.48	13.4	12.1	2.79	1.56
(b) $\mu_0 H_{ac}$ = 20 mT	A (J/kg-Fe)		$\mu_0 H_c$ (mT)		M_r (Am^2/kg-Fe)		M_3 (Am^2/kg-Fe)	
	3 kHz	20 kHz	3 kHz	20 kHz	3 kHz	20 kHz	3 kHz	20 kHz
S1	1.28	2.06	4.32	6.78	49.1	59.7	20.9	19.0
S2	1.40	2.00	4.50	6.69	53.0	60.0	21.2	19.8
S3	1.38	2.01	4.51	6.66	53.4	60.2	21.6	19.9

SAR $= A \bullet f = \pi \mu_0 H_{ac} f M_1^{''}$. We also note that to realize a stable SAR value without being affected by the viscosity, magnetization via the Néel mechanism is suitable. Therefore, we discuss $M_1^{''}$ shown in Fig. 6(b), which was caused by the Néel mechanism. $M_1^{''}$ gradually increased with increasing f in the range $f < f_p$, reached a peak value at $f = f_p$, and then sharply decreased with increasing f in the range $f > f_p$ for the case of $\mu_0 H_{ac} = 20$ mT. This frequency dependence of $M_1^{''}$ means that a relatively large SAR value can be expected even if the excitation frequency f is somewhat lower than f_p. For example, $M_1^{''}$ at $f = 20$ kHz is 67% of the maximum value of $M_1^{''}$ at $f_p = 650$ kHz, even though f is lower than 1/30 of f_p. This indicates that SAR value is approximately proportional to f in the range $f \leq f_p = f_N(H_{ac})$. Therefore, an excitation field with a relatively large amplitude and frequency that satisfies $f_B(H_{ac}) \ll f \leq f_N(H_{ac})$ is suitable for MFH.

Note that large hysteresis cannot be obtained for the case $f \ll f_B(H_{ac}) \ll f_N(H_{ac})$. This is because the magnetization occurs without a phase lag due to the particle rotation via the Brownian mechanism. However, for $f_B(H_{ac}) \ll f$, a large SAR value can be expected since the easy axes of the MNPs are aligned in the direction of the AC excitation field [12,29].

We also note that the values of H_{ac} and f should be increased larger than 20 mT and 20 kHz on condition of $f_B(H_{ac}) \ll f \leq f_N(H_{ac})$ for MFH application. In this case, SAR increases in proportional to $H_{ac} f$.

5. Conclusions

In this study, we investigated the effects of the surrounding viscosity and the excitation field condition on the AC magnetization of MNPs. By measuring the AC magnetization and harmonic magnetization spectra from three samples with different viscosities under different excitation field conditions, we showed that the AC $M - H$ curve and harmonic magnetization spectrum strongly depend on the viscosity for a small excitation field amplitude and low excitation frequency, while they are insensitive to the viscosity for a large excitation field amplitude and high excitation frequency. The differing behaviors can be qualitatively explained when we take the field dependent Brownian and Néel frequencies into account. We note that insensitiveness of the AC magnetization to the viscosity will be useful for MFH and MPI applications because their performances are not affected by the environment viscosity. Finally, we determined the appropriate excitation field condition for MFH from the frequency dependence of the imaginary part of the magnetization via the Néel mechanism.

Acknowledgements

This work was partly supported by the JSPS KAKENHI, Grant numbers JP15H05764 and JP18K04170. We thank Melissa Gibbons, PhD, from Edanz Group (www.edanzediting.com/ac) for editing a draft of this manuscript.

References

[1] Q.A. Pankhurst, N.T.K. Thanh, S.K. Jones, J. Dobson, Progress in applications of magnetic nanoparticles in biomedicine, J. Phys. D 42 (2009) 224001.
[2] R.E. Rosensweig, Heating magnetic fluid with alternating magnetic field, J. Magn. Magn. Mater. 252 (2002) 370–374.
[3] B. Gleich, J. Weizenecker, Tomographic imaging using the nonlinear response of magnetic particles, Nature 435 (2005) 1214–1217.
[4] D. Eberbeck, F. Wiekhorst, S. Wagner, L. Trahms, How the size distribution of magnetic nanoparticles determines their magnetic particle imaging performance, J. Appl. Phys. 98 (2011) 182502.
[5] T. Yoshida, N.B. Othman, T. Tsubaki, J. Takamiya, K. Enpuku, Evaluation of harmonic signals for the detection of magnetic nanoparticles, IEEE Trans. Magn. 48 (2012) 3788–3791.
[6] Y. Higuchi, S. Uchida, A.K. Bhuiya, T. Yoshida, K. Enpuku, Characterization of magnetic markers for liquid-phase detection of biological targets, IEEE Trans. Magn. 49 (2013) 3456–3459.
[7] F. Ludwig, D. Eberbeck, N. Löwa, U. Steinhoff, T. Wawrzik, M. Schilling, L. Trahms, Characterization of magnetic nanoparticle systems with respect to their magnetic particle imaging performance, Biomed. Tech. (Berl). 58 (2013) 535–545.
[8] S. Ota, R. Kitaguchi, R. Takeda, T. Yamada, Y. Takemura, Rotation of magnetization derived from brownian relaxation in magnetic fluids of different viscosity evaluated by dynamic hysteresis measurements over a wide frequency range, Nanomaterials 6 (2016) 170.
[9] C. Shasha, E. Teeman, K.M. Krishnan, Harmonic simulation study of simultaneous nanoparticle size and viscosity differentiation, IEEE Magn. Lett. 8 (2017) 1509405.
[10] B.B. Lahiri, S. Ranoo, A.W. Zaibudeen, J. Philip, Magnetic hyperthermia in magnetic nanoemulsions: effects of polydispersity, particle concentration and medium viscosity, J. Magn. Magn. Mater. 441 (2017) 310–327.
[11] T. Viereck, C. Kuhlmann, S. Draack, M. Schilling, F. Ludwig, Dual-frequency magnetic particle imaging of the Brownian particle contribution, J. Magn. Magn. Mater. 427 (2017) 156–161.
[12] T. Yoshida, S. Bai, A. Hirokawa, K. Tanabe, K. Enpuku, Effect of viscosity on harmonic signals from magnetic fluid, J. Magn. Magn. Mater. 380 (2015) 105–110.
[13] D. Cabrera, A. Lak, T. Yoshida, M.E. Materia, D. Ortega, F. Ludwig, P. Guardia, A. Sathya, T. Pellegrino, F.J. Teran, Unraveling viscosity effects on the hysteresis losses of magnetic nanocubes, Nanoscale 9 (2017) 5094–5101.
[14] T. Yoshida, K. Enpuku, F. Ludwig, J. Dieckhoff, T. Wawrzik, A. Lak, M. Schilling, Characterization of Resovist® nanoparticles for magnetic particle imaging, Springer Proc. Phys. 140 (2012) 1–5.
[15] T. Yoshida, N.B. Othman, K. Enpuku, Characterization of magnetically fractionated magnetic nanoparticles for magnetic particle imaging, J. Appl. Phys. 114 (2013) 173908.
[16] T. Rheinländer, R. Kötitz, W. Weitschies, W. Semmler, Magnetic fractionation of magnetic fuids, J. Magn. Magn. Mater. 219 (2000) 219–228.
[17] N. Löwa, P. Knappe, F. Wiekhorst, D. Eberbeck, A.F. Thünemann, L. Trahms, Hydrodynamic and magnetic fractionation of superparamagnetic nanoparticles for magnetic particle imaging, J. Magn. Magn. Mater. 380 (2015) 266–270.
[18] D.V. Berkov, P. Görnert, N. Buske, C. Gansau, J. Muller, M. Giersig, W. Neumann, D. Su, New method for the determination of the particle magnetic moment distribution in a ferrofluid, J. Phys. D 33 (2000) 331.
[19] J. van Rijssel, B.W.M. Kuipers, B.H. Erné, Non-regularized inversion method from light scattering applied to ferrofluid magnetization curves for magnetic size distribution analysis, J. Magn. Magn. Mater. 353 (2014) 110–115.
[20] K. Enpuku, T. Sasayama, T. Yoshida, Estimation of magnetic moment and anisotropy energy of magnetic markers for biosensing application, J. Appl. Phys. 119 (2016) 184902.
[21] Nian-Sheng Cheng, Formula for the viscosity of a glycerol-water mixture, Ind. Eng. Chem. Res. 47 (2008) 3285–3288.
[22] N. Smith, Reciprocity principles for magnetic recording theory, IEEE Trans. Magn. 231 (1987) 1995–2002.
[23] T. Sasayama, T. Yoshida, K. Tanabe, N. Tsujimura, K. Enpuku, Hysteresis loss of fractionated magnetic nanoparticles for hyperthermia application, IEEE Trans. Magn. 51 (2015) 5101504.
[24] W.T. Coffey, P.J. Cregg, Y.P. Kalmykov, I. Prigogine, S.A. Rice (Eds.), Advances in Chemical Physics, Wiley, New York, 1993, p. 263.
[25] T. Yoshida, Y. Matsugi, N. Tsujimura, T. Sasayama, K. Enpuku, T. Viereck, M. Schilling, F. Ludwig, Effect of alignment of easy axes on dynamic magnetization of immobilized magnetic nanoparticles, Magn. Magn. Mater. 427 (2017) 162–167.
[26] J.L. Déjardin, Y.P. Kalmykov, Nonlinear dielectric relaxation of polar molecules in a strong ac electric field: steady state response, Phys. Rev. E 61 (2000) 1211.
[27] A.L. Elrefai, T. Sasayama, T. Yoshida, K. Enpuku, Magnetic core-size distribution of magnetic nanoparticles estimated from magnetization, AC susceptibility and relaxation measurements, IEEE Trans. Magn 53 (2017) 8204605.
[28] A.L. Elrefai, T. Sasayama, T. Yoshida, K. Enpuku, Empirical expression for DC magnetization curve of immobilized magnetic nanoparticles for use in biomedical applications, AIP Adv. 8 (2018) 056803.
[29] H. Mamiya, B. Jeyadevan, Hyperthermic effects of dissipative structures of magnetic nanoparticles in large alternating magnetic fields, Sci. Rep. 1 (2011) 157.